Phenotype-based high-content chemical library screening identifies statins as inhibitors of in vivo lymphangiogenesis

Martin Michael Peter Schulz[a], Felix Reisen[a], Silvana Zgraggen[a], Stephanie Fischer[a], Don Yuen[b], Gyeong Jin Kang[b], Lu Chen[b], Gisbert Schneider[a], and Michael Detmar[a,1]

[a]Institute of Pharmaceutical Sciences, Swiss Federal Institute of Technology, Eidgenössische Technische Hochschule Zurich, Wolfgang-Pauli-Strasse 10, 8093 Zurich, Switzerland; and [b]Center for Eye Disease and Development, Program in Vision Science and School of Optometry, University of California, 689 Minor Hall, Berkeley, CA 94720

Lymphangiogenesis plays an important role in promoting cancer metastasis to sentinel lymph nodes and beyond and also promotes organ transplant rejection. We used human lymphatic endothelial cells to establish a reliable three-dimensional lymphangiogenic sprouting assay with automated image acquisition and analysis for inhibitor screening. This high-content phenotype-based assay quantifies sprouts by automated fluorescence microscopy and newly developed analysis software. We identified signaling pathways involved in lymphangiogenic sprouting by screening the Library of Pharmacologically Active Compounds (LOPAC)^{1280} collection of pharmacologically relevant compounds. Hit characterization revealed that mitogen-activated protein kinase kinase (MEK) 1/2 inhibitors substantially block lymphangiogenesis in vitro and in vivo. Importantly, the drug class of statins, for the first time, emerged as potent inhibitors of lymphangiogenic sprouting in vitro and of corneal and cutaneous lymphangiogenesis in vivo. This effect was mediated by inhibition of the 3-hydroxy-3-methylglutaryl-coenzyme A (HMG-CoA) reductase and subsequently the isoprenylation of Rac1. Supplementation with the enzymatic products of HMG-CoA reductase functionally rescued lymphangiogenic sprouting and the recruitment of Rac1 to the plasma membrane.

high-content screening | small compound screening | lymphatic endothelium | chemical genetics

Cancer metastasis accounts for the majority of cancer patients' deaths. The lymphatic vascular system drains interstitial fluids and cells to the lymph nodes and also serves as a major route for disseminating cancer cells. Indeed, the tumor-draining sentinel lymph node represents the first site of metastasis in the majority of epithelial cancers and malignant melanomas (1), and the presence of sentinel lymph node metastases is an important negative prognostic indicator and also has an impact on the choice of cancer therapy. While the lymphatic vascular system has traditionally been thought to only play a passive role in cancer metastasis, with preexisting lymphatic vessels serving as mere conduits for invading tumor cells, there is increasing evidence that malignant tumors can actively induce the growth of lymphatic vessels. This process, termed tumor lymphangiogenesis, has been found to promote metastatic spread to sentinel lymph nodes and beyond (1). Increased tumor lymphangiogenesis is positively correlated with an increased incidence of sentinel lymph node metastasis and with reduced overall survival in several types of human cancers (1, 2). Importantly, tumor-induced lymphangiogenesis also occurs in the tumor-draining sentinel lymph nodes, sometimes even before metastatic spread (3). Lymph node lymphangiogenesis might provide a metastatic niche for cancer cells, possibly including tumor-initiating cancer stem cells, and might promote further metastatic cancer spread (4). Recently, lymphangiogenesis has also been found to promote alloreactive immune responses and rejection in renal transplants, corneal grafts, and lung transplants (5).

The vascular endothelial growth factors (VEGFs) VEGF-C, VEGF-D, and VEGF-A have been found to potently promote tumor lymphangiogenesis and lymphatic metastasis (3, 6, 7), as well as lymphangiogenesis in other pathological settings, interacting with VEGF receptors (VEGFRs) -2 and -3. Blockade of VEGF receptors, in particular of the VEGF-C/VEGFR-3 pathway, resulted in a reduction of lymphatic metastases and of corneal transplant rejections in several experimental models (5). More recently, blockade of the neuropilin-2 receptor on activated lymphatic endothelium was reported to also reduce lymphatic cancer metastasis (8). Overall, however, the inhibitory effects observed in these studies were only partial or temporary, and there is an urgent need for the identification of novel targets for the therapeutic inhibition of lymphangiogenesis.

The formation of lymphatic vessel sprouts is one of the first and essential steps in the development of new lymphatic vessels. To initiate lymphangiogenesis, selected tip cells from the wall of preexisting vessels send out protrusions and sprout into the extracellular matrix on their basolateral site. This process is analogous to the first steps of blood vessel angiogenesis (9) and integrates several mechanistic steps including cell–cell communication with neighboring cells, cell polarization, matrix degradation, migration, and invasion. Therefore, to identify signaling pathways involved in lymphangiogenesis and potential inhibitors of lymphangiogenesis, we selected lymphatic sprout formation as the readout for the development of a phenotype-based, high-content screening assay for the screening of chemical libraries. Compared to target-based screens, the observation of a distinct phenotype in response to drug treatment allows to link the drug effect to physiologically relevant processes. The success rate of phenotype-based approaches for the discovery of first-in-class small molecules was higher than that of target-based approaches between 1999 and 2008 (28 vs. 17), even though most screening endeavors were target-based (10). Phenotype-based drug discovery is also thought to result in fewer failed drugs (10).

In this study, we used human dermal microvascular lymphatic endothelial cells (LECs) to establish a reliable three-dimensional (3D) lymphangiogenic sprouting assay with automated image acquisition and analysis, as a phenotypic screening assay for

inhibitors of lymphangiogenesis. In addition to the identification of many small molecules previously not described as anti-lymphangiogenic, we also characterized the anti-lymphangiogenic effects of statins with potential implication for their clinical use.

Results

Development and Validation of an Automatable Phenotype-based Lymphangiogenic Sprouting Assay. We set out to develop an automatable 3D in vitro system for quantification of sprout formation by human LECs. Whereas spheroid cultures (aggregates of endothelial cells) have been widely used for analyses of sprout formation, we found that the coating of cytodextran microcarrier beads with human LECs required lower cell numbers, yielded more uniform results, and was easier to handle when compared to the establishment of LEC spheroids. LEC-coated beads were embedded into hydrogels to enable sprout formation in a 3D environment (Fig. 1). When compared to fibrin gels, we found that collagen type I gels were easier to set up, polymerized readily at 37 °C, and yielded greater sprout numbers. Time course studies revealed that sprout formation was clearly detectable after 24 h, with no major increase after 48 h and a reduction after 72 h. Thus, the 24 h time point was chosen for all further analyses.

Before gel encapsulation, LEC-coated beads had dense monolayer coverage with fluorescently labeled LECs. These LECs displayed a characteristic endothelial morphology and membrane-bound CD31 staining (Fig. 2A). At 24 h after encapsulation, cellular protrusions sprouted into the surrounding collagen matrix (Movie S1). To achieve single-sprout resolution at all levels on the epifluorescence screening microscope, six-layer z-projections were acquired covering the whole bead and resolving all sprouts (Fig. 2B). For quantitative analysis of sprout formation, we determined the sprout number per bead, which was easier to acquire than cumulated or average sprout length, but yielded a similarly wide assay window.

Since we aimed at identifying inhibitors of lymphangiogenesis by chemical compound library screening, we first investigated which factors present in many tumor microenvironments might promote LEC sprout formation in our assay. After 24 h of treatment, VEGF-A moderately promoted lymphangiogenic sprouting (0.20 sprouts/bead compared to 0.08 sprouts/bead with medium only; $p < 0.05$; Fig. 2C). Basic fibroblast growth factor (bFGF) and sphingosine-1-phosphate (S1P) alone did not significantly promote sprouting (0.17 sprouts/bead and 0.12 sprouts/bead, respectively; not significant), whereas a combination of bFGF with S1P increased sprouting to a similar degree as VEGF-A alone (0.25 sprouts/bead; $p < 0.05$). Combining VEGF-A with either S1P or bFGF strongly promoted LEC sprouting (0.56 sprouts/bead and 0.59 sprouts/bead, respectively; both $p < 0.001$). Combining VEGF-A with bFGF and S1P ("sprouting inducer mix") yielded the strongest sprouting response (0.75 sprouts/bead; $p < 0.001$) and was therefore used for compound screening. Addition of the VEGF receptor tyrosine kinase inhibitor sunitinib reduced the sprouting activity induced by the sprouting inducer mix by 88.6% (Fig. 2 C and D). Thus, for all screens, sunitinib was used as a positive control. Taken together, these results confirmed that the chosen assay conditions were indeed suitable to identify drug-like compounds that inhibit lymphatic sprouting.

Automation of the Phenotype-based Lymphangiogenic Sprouting Assay. While the assay setup and compound treatment were performed manually, the actual screening [with a throughput of up to 1,500 compounds per day (Fig. 1 A–C)], image acquisition, and analysis were fully automated (Fig. 1 D and E). Sprout formation was measured by automated epifluorescence imaging and counting of fluorescently labeled cell protrusions into the collagen matrix. To vertically visualize all sprouts originating from different positions on the bead, six layers spanning the whole diameter of the bead (133–215 μm) were acquired with an increment of
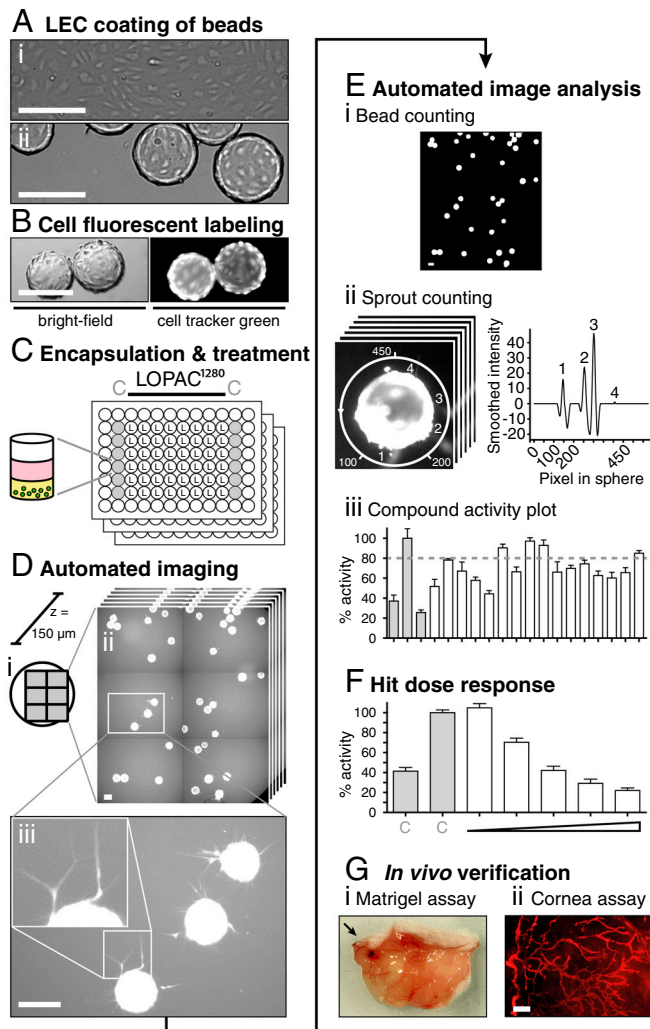

Fig. 1. Strategy for the identification and profiling of inhibitors of lymphangiogenic sprouting in a high-content-screen. (A) Phase-contrast micrographs show cultured LECs as confluent 2D monolayers (i) and after coating onto beads as sprouting sources (ii). (B) Beads (green circles) were fluorescently labeled with cell tracker green (CTG), (C) encapsulated into collagen hydrogels (yellow), and cultured with medium (pink) supplemented with control (C) or LOPAC test compounds at 5 μM in a 96-well format. (D) Automated fluorescent scanning of plates resulted in 2 × 3 tile scans representing 80% of each well surface (i). Scans were acquired in six layers spanning the whole bead depth (150 μm) with an increment of 30 μm (ii). 24 h after treatment, LEC-coated beads showed cellular protrusions that sprouted into the collagen gel (iii). (E) Sprout number per bead was calculated by our in-house developed software SproutCounter. Beads were detected by thresholding and subsequent cluster analysis (i) and sprouts were counted by applying a sphere around the selected beads and measuring pixel intensities (Materials and Methods, Figs. S1–S3) (ii). Results are presented as "% activity compared to negative control" with an 80% cutoff defining inhibitors (iii). (F) Selected hits were reordered, retested under identical conditions, and profiled by dose response measurements, (G) before testing in two in vivo mouse models. Scale bars represent 200 μm.

30 μm. A tile scan spanning 80% of the well surface was applied for horizontal visualization of a maximal number of beads (Fig. 1D). In total, 54 96-well plates were imaged within 36 h, generating 116,640 images. The assay readout—i.e., sprout number per bead—was quantified by our in-house developed software SproutCounter (Fig. 1E; for more detail, cf. Figs. S1–S3 and SI Materials and Methods). First, beads were identified by adaptive thresholding and subsequent high pixel-intensity clustering (Fig. 1E, i). Then, pixel intensities were measured along spheres that were placed around the so-identified beads. This
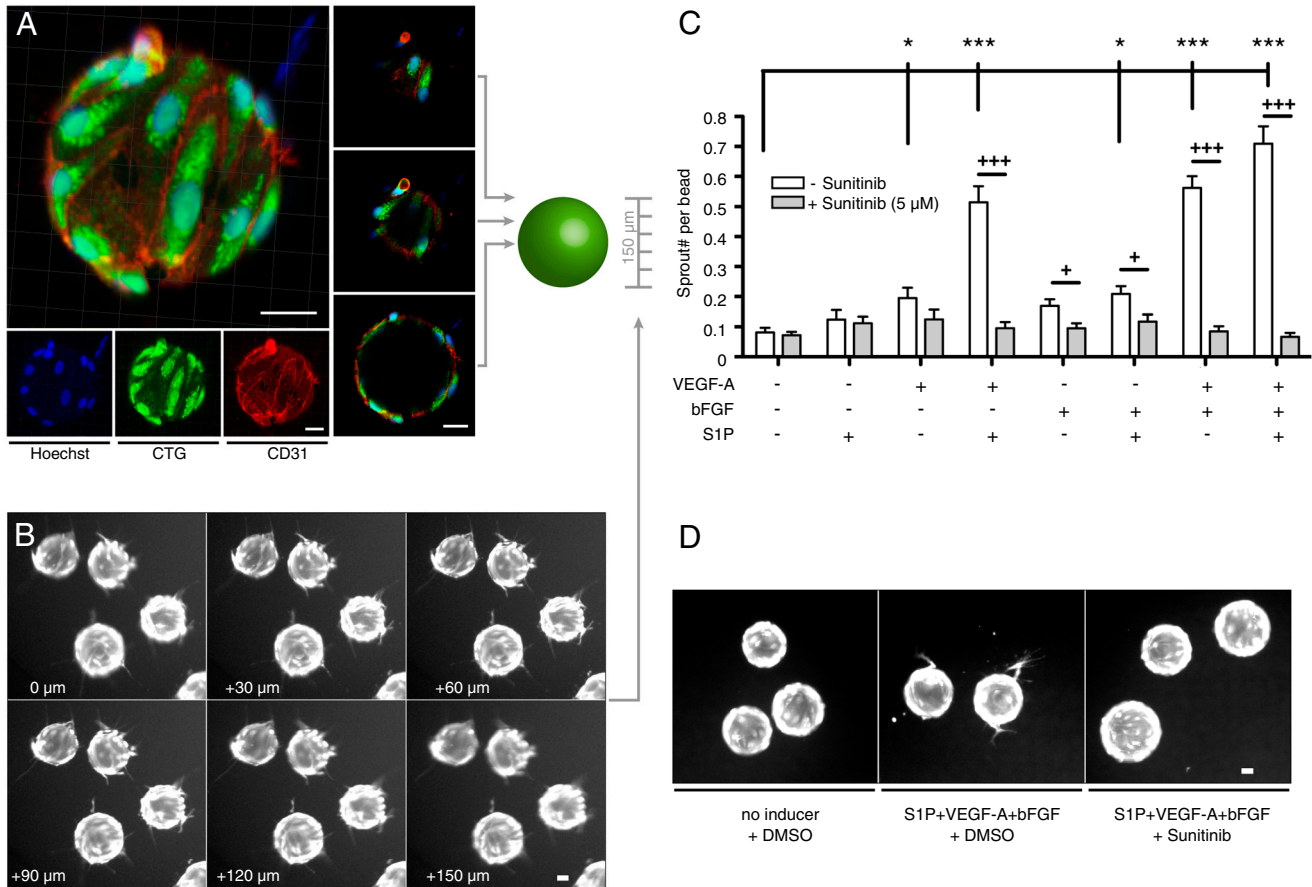
Fig. 2. Sprouting assay validation. (A) Confocal imaging of LEC bead coverage by immunofluorescent CD31 staining (red), cytosolic labeling with CTG dye (green), and nuclear labeling with Hoechst dye (blue) demonstrates a dense LEC population with characteristic cell-cell contacts in a maximum intensity projection (left panel) and optical cross-sections (central panel). (B) Fluorescence images of CTG-labeled sprouting LECs show the existence and visualization of sprouts in all scanned layers. (C) Sprouting response as sprout number per bead measured for different combinations of lymphangiogenic stimulants in the sprouting assay. A combination of 40 ng/ml VEGF-A, 40 ng/ml bFGF, and 2 µM S1P yielded the strongest sprouting response that was inhibited after addition of the receptor tyrosine kinase inhibitor sunitinib (5 µM). (D) Representative images of sprouting beads from panel C show pronounced CTG positive protrusions in S1P+VEGF-A+bFGF treated wells but not in S1P+VEGF-A+bFGF+sunitinib or untreated wells. */**/*** $p < 0.05/0.01/0.001$ in one-way ANOVA with simple "contrast" post test. +/++/+++ $p < 0.05/0.01/0.001$ in unpaired Student t-tests. $n = 10$. Bars show mean ± SEM. All scale bars represent 30 µm.

resulted in intensity vectors whose peak numbers served as estimate for the number of sprouts per bead (Fig. 1E, ii). The sprout number per bead data was normalized as percentage activity compared to the negative control (DMSO vehicle; Fig. 1E, iii).

To investigate the versatility of the 3D bead assay and its automated quantification for applications beyond lymphangiogenesis, we modified the setup to establish a cancer invasion assay. To this end, we coated beads with MDA-MB-231 mammary carcinoma cells that were encapsulated into collagen type I gels and incubated with VEGF-A and bFGF for 24 h. We found that MDA-MB-231 cells readily invaded the surrounding gel and that the number of invading cells was markedly reduced by addition of sunitinib (Fig. S4A). After moderate parameter adjustments, the SproutCounter software was able to quantify and clearly separate the positive and negative control for this invasion assay (Fig. S4B).

Identification of Lymphangiogenic Sprouting Inhibitors by LOPAC[1280] Screening. To identify pathways involved in lymphangiogenesis and potential lymphangiogenic inhibitors, we tested the small compound Library of Pharmacologically Active Compounds (LOPAC)[1280] in the 3D sprouting assay. We found a good intraplate separation between the positive (sunitinib) and the negative (DMSO vehicle) control (Fig. S5 A and B) with an averaged signal-to-noise ratio over all plates of 4.7 ± 0.4 for replicate 1 and 7.2 ± 0.7 for replicate 2 (Fig. S3D). The number of sprouts per bead was normalized to the intraplate negative control and expressed as percent activity (Fig. 3A). An inter-replicate variability of less than 30% was found for 85.8% of all tested drugs, indicating the screen reproducibility (Fig. S5D). The top hit rate, defined by at least a 20% inhibition in both replicates, was 2.4% (31 compounds of 1,280; Table 1). Among these compounds, 32.3% (10 compounds) were cytotoxic drugs, interfering with DNA metabolism, cytoskeleton and ECM, or apoptosis inducers, such as taxol, colchicine, and idarubicin. Visual inspection of the images obtained after treatment with these compounds confirmed their cytotoxic effect and sprouting inhibition (Fig. 3E and Fig. S5C). Treatment with the topoisomerase II inhibitor idarubicin resulted in LEC removal from the bead surface and necrotic cell appearance (Fig. S5C). In contrast, treatment with mevastatin or U0126, two other hits from the primary screen, did not influence LEC attachment and bead coverage but reduced the number of outgrowing sprouts compared to vehicle treatment (Fig. 3E).

Nine compounds (29.0% of the top hits) had been identified as inhibitors of angiogenesis and lymphangiogenesis in previous screens, namely semaxanib (SU 5416), a predecessor of sunitinib, indirubin-3'-oxime, podophyllotoxin, ammonium pyrrolidine-dithiocarbamate, IC 261, 7-chloro-4-hydroxy-2-phenyl-1,8-naphthyridine, tetraethylthiuram disulfide, emetine dihydrochloride hydrate, and 7-cyclopentyl-5-(4-phenoxy)phenyl-7H-pyrrolo[2,3-d]pyrimidin-4-ylamine. Three of the remaining 13 top hits (9.7% of the top hits) were dopamine antagonists that are abun-
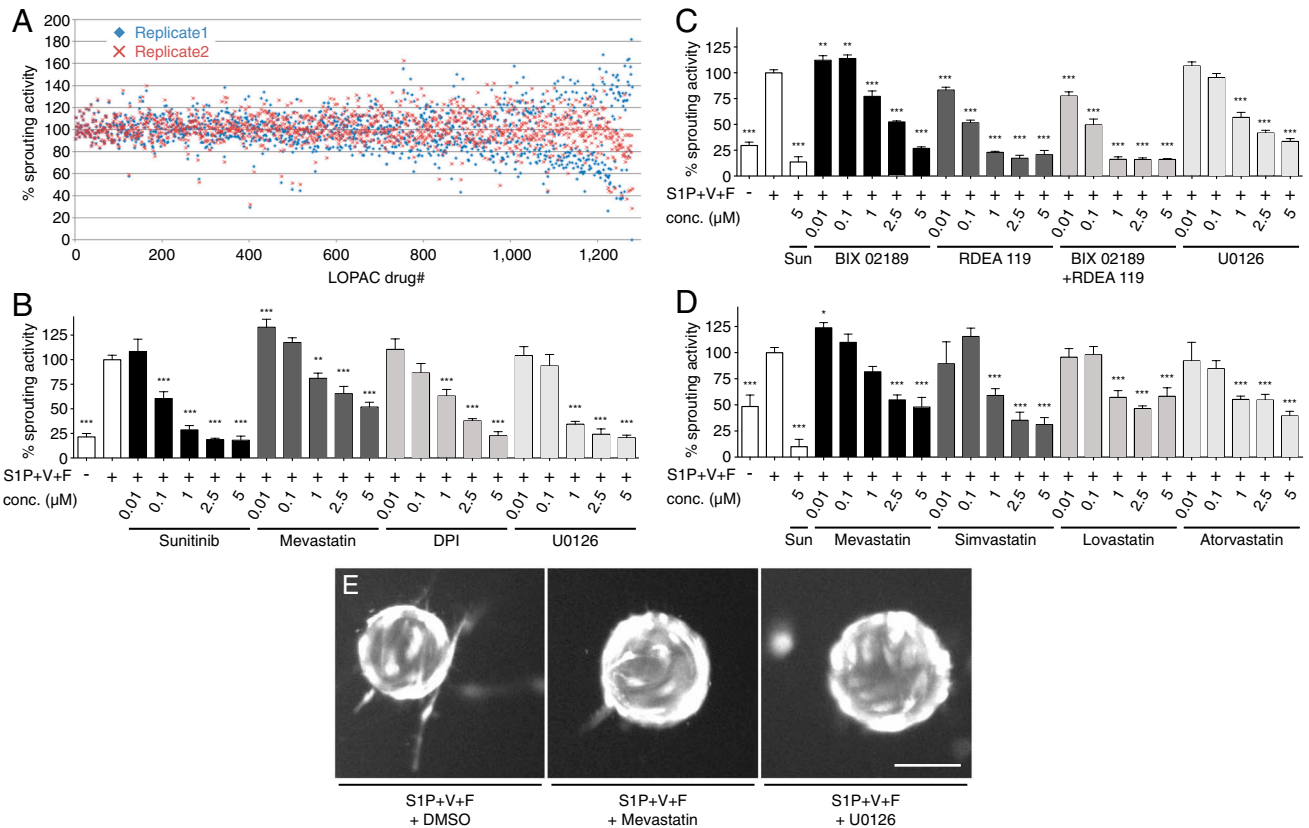
Fig. 3. Drug activity screening result and dose dependence. (*A*) 1,280 LOPAC compounds are plotted for their activity compared to negative control. The screen was repeated once (replicate 1 in blue diamonds, replicate 2 in red crosses). Drugs are sorted from left to right with increasing difference between replicate 1 and replicate 2 (inter-replicate variability) that was less than 30% for 85.8% of all drugs (see also Fig. S5*D*). (*B*) Selected hits were reordered and retested in the LEC sprouting assay in quintuplicates in three repetitions. Mevastatin, diphenyleneiodonium chloride (DPI), and the MEK inhibitor U0126 showed a dose dependent inhibition of lymphangiogenic sprouting. Sunitinib (Sun) was used as positive control. (*C*) The MEK1/2 specific inhibitor RDEA 119 decreased lymphangiogenic sprouting in a dose dependent manner more potently than the MEK5 specific inhibitor BIX 01289. (*D*) Besides mevastatin, three other statins also inhibited lymphangiogenic sprouting dose dependently. (*E*) Representative frames of the screening-acquired images are shown, reflecting the cell viability by visual morphological assessment. Treatment with the screening hits mevastatin and U0126 did not compromise the LEC bead coverage and morphology but reduced the sprout number compared to DMSO treatment. Scale bar represents 100 μm. $S1P + V + F = S1P(2\ \mu M) + VEGF\text{-}A(40\ ng/ml) + bFGF(40\ ng/ml)$. */**/*** $p < 0.05/0.01/0.001$ in one-way ANOVA with simple "contrast" post-test. Bars show mean ± SEM.

dant (8.8%) in the LOPAC library. The remaining 10 top hits included inhibitors of important cellular pathways, such as the MEK1/2 inhibitor U0126, the PDGF receptor inhibitor tyrphostin A9, the EGF receptor inhibitor tyrphostin 47, the insulin-like growth factor 1 inhibitor tyrphostin AG 538, the PI3K inhibitor wortmannin, and a PKC-α inhibitor dequalinium analog. Among the 31 top hits we found 10 annotated kinase inhibitors (32.3%), which corresponds to an enrichment factor of 4.7 when compared to the background frequency of 6.8% in the (LOPAC)[1280] that contains 87 kinase inhibitors.

Based on the observed inhibition of lymphatic sprouting (Table 1) and literature research for potential mechanisms and novelty, U0126, a MEK inhibitor, diphenyleneiodonium chloride (DPI), an eNOS inhibitor, and mevastatin were selected for further studies. While U0126 and DPI fulfilled the top hit inclusion criteria (>20% sprouting inhibition compared to negative control) in both replicates, mevastatin, the only statin in the (LOPAC)[1280], complied in only one of the two replicates with this threshold but was chosen for the high medical impact of the statins. The compounds were reordered and tested in dose-response experiments with higher replicate numbers (Fig. 1*F*). All three tested drugs were found to have a dose-dependent inhibitory effect on lymphangiogenic sprouting, with a minimal effective concentration of 1 μM (Fig. 3*B*).

MEK Inhibitor U0126 Inhibits Lymphangiogenesis in Vitro and in Vivo. U0126 has been described as a MEK1/2 inhibitor (11). We inves-

tigated whether its sprouting inhibitory effect is conveyed via inhibition of MEK1/2, its primary target, or by inhibition of MEK5 for which U0126 has a side-specificity at higher concentrations (11). Therefore, the MEK1/2 specific inhibitor RDEA 119, and the MEK5 specific inhibitor BIX 02189 were tested alone or in combination. While BIX 02189 alone inhibited lymphangiogenic sprouting with a minimal effective concentration of 1 μM, RDEA 119 was more potent with a minimal effective concentration of 10 nM (Fig. 3*C*). The combination of both compounds did not result in increased inhibition. Treatment of LECs with 5 μM U0126 in the presence of S1P+VEGF-A+bFGF reduced phosphorylation of MEK1/2's only substrate ERK1/2 to a level comparable to the control without addition of S1P+VEGF-A+bFGF (Fig. 4*A*). The minimal effective concentration needed for inhibition of lymphangiogenic sprouting (1 μM) was much lower than the minimal effective concentration needed for inhibition of proliferation (30 μM) (Fig. 4*B*).

We next investigated whether U0126 might also inhibit lymphangiogenesis in vivo. To this end, we tested its efficacy in the established mouse Matrigel plug assay, in which a growth-factor-containing gel is implanted subcutaneously (12). Daily treatment with U0126 (15 mg/kg body weight) by intraperitoneal injection resulted in fewer CD31^{+}/LYVE-1^{+} lymphatic vessels in the dermis adjacent to the growth-factor-loaded Matrigel when compared to vehicle treatment (Fig. 5*A*). Quantitative image analyses of immunostained tissue sections revealed that U0126 treatment completely prevented lymphangiogenesis induced by

Table 1. LOPAC[1280] screening top hit list

Compounds	Pharmacol. class	Selectivity	R 1	R 2	Avrg.	Rank
			% activity		
Sanguinarine chloride	Ion Pump	Na^+/K^+ ATPase	0.0	28.5	14.3	1
Calcimycin	Intracellular Calcium	Ca^{2+}	29.5	32.1	30.8	2
Indirubin-3'-oxime	Phosphorylation	CDK	26.3	47.0	36.7	3
Podophyllotoxin	Cytoskeleton and ECM		44.8	50.2	47.5	4
Mitoxantrone	DNA Metabolism		46.0	51.3	48.6	5
Tyrphostin A9	Phosphorylation	PDGFR	43.5	54.5	49.0	6
(S)-(+)-Camptothecin	Apoptosis	TopoI	63.4	37.1	50.3	7
Ammonium pyrrolidinedithiocarbamate	Nitric Oxide	NOS	57.4	44.6	51.0	8
IC 261	Phosphorylation	CK-1delta/epsilon	63.3	40.2	51.8	9
Colchicine	Cytoskeleton and ECM	Tubulin	43.5	60.9	52.2	10
7-Chloro-4-hydroxy-2-phenyl-1,8-naphthyridine	Adenosine	A1	55.1	52.1	53.6	11
Tetraethylthiuram disulfide	Biochemistry	Alcohol Dehydrogenase	63.9	43.4	53.7	12
Brefeldin A from Penicillium brefeldianum	Cytoskeleton and ECM	Golgi apparatus	64.6	44.6	54.6	13
Taxol	Cytoskeleton and ECM	Tubulin	51.9	57.6	54.7	14
Emetine dihydrochloride hydrate	Apoptosis		60.7	49.1	54.9	15
Idarubicin	DNA Metabolism		44.1	69.6	56.8	16
Tomoxetine	Adrenoceptor	Reuptake	57.6	59.0	58.3	17
Dequalinium analog, C-14 linker	Phosphorylation	PKC-alpha	70.9	46.7	58.8	18
Dihydroouabain	Ion Pump	Na^+/K^+ Pump	75.8	44.1	59.9	19
Tyrphostin AG 538	Phosphorylation	IGF-1 RTK	65.2	54.8	60.0	20
Diphenyleneiodonium chloride	Nitric Oxide	eNOS	50.7	70.5	60.6	21
Thapsigargin	Intracellular Calcium		55.3	68.9	62.1	22
Tyrphostin 47	Phosphorylation	EGFR	66.6	61.5	64.1	23
N-Oleoyldopamine	Neurotransmission	CB1	62.0	70.2	66.1	24
7-Cyclopentyl-5-(4-phenoxy)phenyl-7H-pyrrolo[2,3-d]pyrimidin-4-ylamine	Phosphorylation	lck	57.2	76.5	66.9	25
U0126	Phosphorylation	MEK1/MEK2	61.9	74.8	68.4	26
SU 5416	Phosphorylation	VEGFR PTK	79.5	60.1	69.8	27
Fluspirilene	Dopamine	D2/D1	75.4	70.5	73.0	28
Propionylpromazine hydrochloride	Dopamine	D2	76.5	72.4	74.4	29
U-99194A maleate	Dopamine	D3	73.5	77.7	75.6	30
Wortmannin from Penicillium funiculosum	Phosphorylation	PI3K	78.4	75.6	77.0	31

Compound name, pharmacological class and selectivity annotations are taken from the (LOPAC)[1280] list. R 1/2 = screening replicate 1/2. % activity = relative sprout number per bead compared to negative control, <80% in both replicates demarks a top hit. Top hit rate 2.4%.

S1P+VEGF-A+bFGF [5.4 versus 10.5 lymphatic vessels/mm epidermal basement membrane (Fig. 5B); lymphatic vessel density in the dermis 1.1% versus 2.7% (Fig. 5D); $p < 0.001$]. These values were comparable to those observed in the skin of mice with growth-factor-free Matrigel implants (5.8 lymphatic vessels/mm epidermal basement membrane; lymphatic vessel density in the dermis 1.1%). The average size of lymphatic vessels was unchanged (Fig. 5C).

Statins Inhibit Lymphangiogenesis in Vitro and in Vivo. To investigate whether the inhibitory effect of mevastatin was also observed with other members of the statin drug class, we tested three commonly used statins along with mevastatin. We found that simvastatin, lovastatin, and atorvastatin dose-dependently inhibited lymphangiogenic sprouting in vitro, with a minimal effective concentration of 1 μM (Fig. 3D). In some experiments, there was a slight increase in sprouting after 0.01 μM mevastatin treatment (Fig. 3 B and D). However, this was not consistently seen and none of the other statins promoted sprouting at low concentrations. Simvastatin displayed the strongest sprouting inhibition and its effects were therefore characterized in more detail. Unlike the VEGFR-2 inhibitor sunitinib or the MEK1/2 inhibitor U0126, simvastatin treatment did not inhibit phosphorylation of VEGFR-2 or ERK (Fig. 4A). LEC proliferation was not inhibited at concentrations below 10 μM (Fig. 4C), while pronounced morphological changes, namely cell body elongation, were already observed at concentrations as low as 1 μM (Fig. 4D), indicating possible effects on the cytoskeleton.

The major target of the statins is 3-hydroxy-3-methylglutaryl-coenzyme A reductase (HMGCR). Therefore, we next investigated whether HMGCR was expressed in LECs in our recently published LEC microarray data. We found that HMGCR is expressed in human dermal microvascular LECs that were used for this study (13) and also in murine intestinal LECs (14). Mevalonate, the product of HMGCR, and its derivatives farnesyl pyrophosphate (FPP) and geranylgeranyl pyrophosphate (GGPP) build the basis for cholesterol synthesis. They are also indispensible for the isoprenylation of monomeric G-proteins to allow their localization to the plasma membrane and their activation. We found that addition of mevalonate, FPP, or GGPP indeed restored simvastatin inhibited lymphangiogenic sprouting to non-simvastatin treated levels and beyond (Fig. 4E).

Rac1 is a monomeric G-protein requiring isoprenylation and is involved in lamellipodia formation. We next investigated the activation of Rac1 and its membrane localization, which is a prerequisite for effective signal transduction. We found that the localization of Rac1 to the plasma membrane was inhibited by simvastatin and that it was rescued by supplementation with mevalonate or FPP (Fig. 4F). Simvastatin also strongly reduced the amount of activated GTP-bound Rac1 compared to control (Fig. 4G).

To investigate whether simvastatin might also exert anti-lymphangiogenic effects in vivo, we employed two murine experimental lymphangiogenesis models. In the Matrigel plug assay, daily i.p. administration of simvastatin (2 mg/kg body weight) resulted in a strong reduction of $CD31^+/LYVE-1^+$ dermal lymphatic vessels when compared to vehicle treatment (Fig. 5A). Quantitative image analyses revealed that the induction of lymphangiogenesis in the vicinity of growth factor-containing Matrigels (S1P+VEGF-A+bFGF) was completely prevented by simvastatin treatment (Fig. 5 B and D; $p < 0.001$). The number of lymphatic vessels and their density in the dermis was comparable
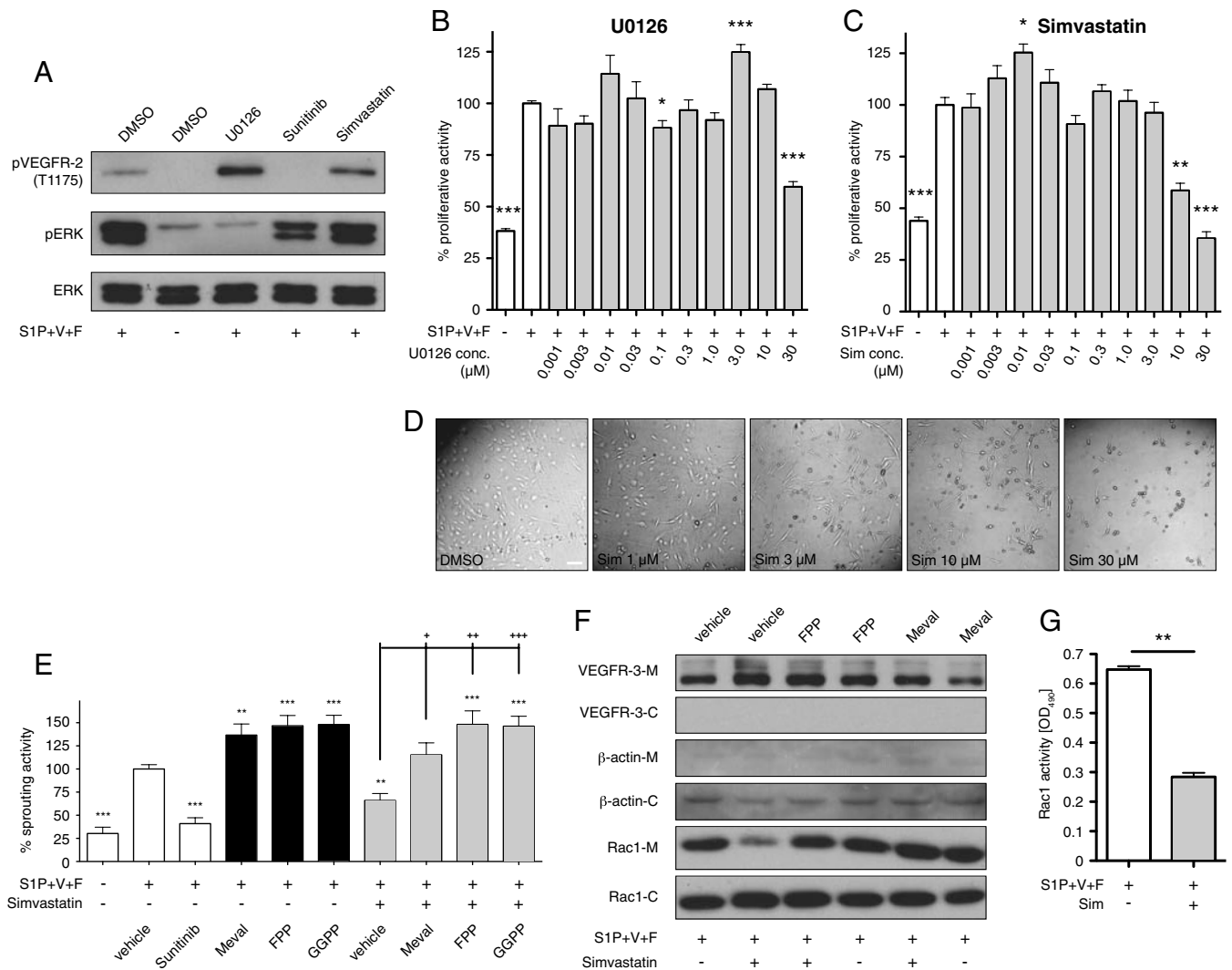
Fig. 4. Mechanism of U0126 and statin mediated inhibition of lymphangiogenic sprouting. (A) LECs were induced with 2 μM S1P, 40 ng/ml VEGF-A, and 40 ng/ml bFGF (S1P+V+F) and treated with 5 μM U0126, sunitinib (Sun), simvastatin (Sim), or equal amounts of vehicle (DMSO). PhosphoVEGFR-2, phosphoERK1/2, and total ERK1/2 levels were measured by Western blotting revealing ERK phosphorylation inhibition by U0126, VEGFR-2 phosphorylation inhibition by sunitinib, and no effect by simvastatin. (B and C) Proliferation of S1P+V+F induced LECs was measured after 48 h treatment with increasing concentrations of U0126 or simvastatin and (D) micrographs were acquired demonstrating an altered LEC morphology by simvastatin and minimal effective concentrations of 10 μM and 30 μM by simvastatin and U0126, respectively, on LEC proliferation. */**/*** $p < 0.05/0.01/0.001$ in unpaired Student t-tests ($n = 5$). (E) HMG-CoA reductase products mevalonate (Meval), farnesyl pyrophosphate (FPP), and geranylgeranyl pyrophosphate (GGPP) rescued simvastatin inhibited LEC sprouting. */**/*** and +/++/+++ $p < 0.05/0.01/0.001$ in one-way ANOVA with simple "contrast" post test ($n = 5$). (F) Separation of membrane (-M) and cytosol (-C) by ultracentrifuge cell fractionation and subsequent Western blotting demonstrates high fraction purity by the absence of the LEC surface receptor VEGFR-3 from the cytosolic fraction and of the cytosolic β-actin from the membrane fraction. 5 μM simvastatin markedly reduced Rac1 levels in the plasma membrane, which was rescued by FPP or mevalonate supplementation. (G) G-LISA measurements showed a reduction of activated GTP-bound Rac1 when treated with 5 μM simvastatin. ** $p < 0.01$ in unpaired Student t-tests ($n = 2$). Scale bar represents 100 μm. Bars show mean ± SEM.

to that observed in the skin of growth factor-free Matrigel implanted animals. Lymphatic vessel size was unaffected by simvastatin treatment (Fig. 5C).

We next studied the effects of simvastatin on the inflammation-induced ingrowth of lymphatic vessels into the avascular cornea in adult mice, an established model of postnatal lymphangiogenesis (15). Treatment with simvastatin (2 mg/kg body weight) resulted in a strong reduction of LYVE-1-positive lymphatic vessels in the cornea when compared with vehicle treatment (Fig. 5E). Quantification of the corneal area that was covered by LYVE-1-positive lymphatic vessels revealed a 47.3% inhibition of corneal lymphangiogenesis after simvastatin treatment (Fig. 5F; $p < 0.05$).

Discussion

In this study, we developed and successfully applied an automated phenotypic in vitro screening assay to identify small molecule inhibitors and pathways involved in lymphangiogenesis. Previously, several studies were performed based on in vitro compound screens with blood vascular endothelial cells, including proliferation assays of human umbilical vein endothelial cells (HUVEC) (16), HUVEC/vascular smooth muscle cell cocultures, human microvascular endothelial cell tube formation assays (17, 18), and HUVEC spheroid sprouting assays (19). While the tube formation assay has been considered as a model of vasculogenesis rather than angiogenesis (20), the other assays attempt to measure different aspects of blood vessel formation. However, a number of studies from our group as well as from other investigators have clearly demonstrated that lymphatic endothelial cells differ from blood vascular endothelial cells with regard to their morphology, differentiation, and function, as well as to the molecular mechanisms inducing their growth (lymphangiogenesis and angiogenesis, respectively) (5).
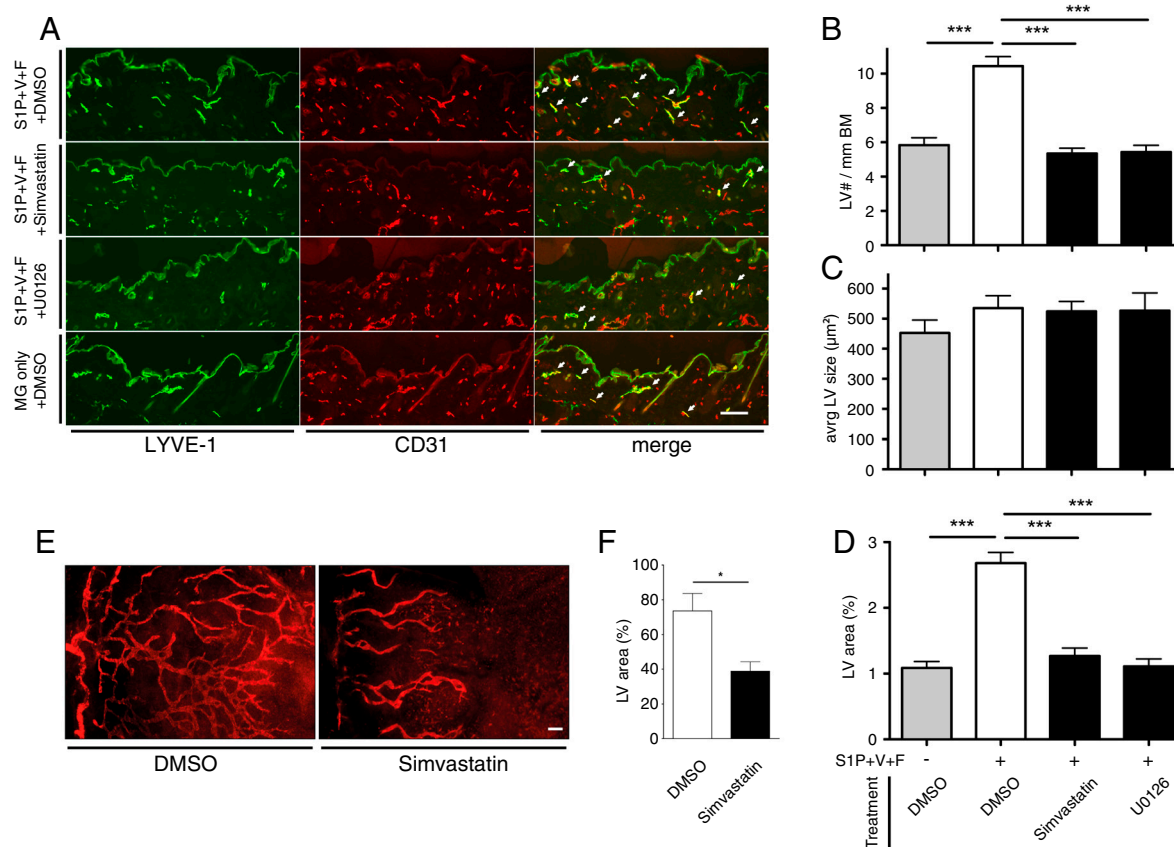
Fig. 5. Simvastatin and U0126 suppress lymphangiogenesis in vivo. (*A*) Representative images of immunofluorescent stains reveal a lower density of lymphatic vessels, which are LYVE-1/CD31 double positive (white arrows) in the dermis overlying the implanted Matrigel plug. The lymphatic vessel (LV) number per mm epidermal basement membrane (BM, the interface between epidermis and dermis) (*B*) and the percent of dermal area covered by lymphatic vessels (*D*) were strongly reduced in simvastatin (2 mg/kg) and U0126 (15 mg/kg) treated mice compared to DMSO vehicle treated mice. No change in LV size was observed (*C*). S1P + V + F = S1P(2 μM) + VEGF-A(500 ng/ml) + bFGF(500 ng/ml) in Matrigel (MG). *** $p < 0.001$ in unpaired Student t-tests (seven animals with two plugs per group). (*E*) Representative micrographs of immunofluorescent LYVE-1 stains labeling lymphatic vessels and quantitative image analyses of LYVE-1 stains (*F*) reveal that simvastatin treatment significantly inhibited corneal lymphangiogenesis induced by suture placement (eight mice per group). * $p < 0.05$ in Mann-Whitney test. LV = lymphatic vessel. Scale bars represent 100 μm. Bars show mean ± SEM.

Thus, we have used human primary LECs and have developed an assay that, in a reductionist manner, without interference of other cell types, measures an initial and crucial step of pathological in vivo lymphangiogenesis, namely sprout formation in a 3D environment. Endothelial sprouting includes tip cell selection and polarization, matrix degradation and invasion (9, 21). It has been extensively studied in blood vascular endothelial cells over the last 15 y, and many findings from in vitro sprouting studies have been confirmed in vivo (22, 23). For lymphatic endothelium, recent findings indicate a role of VEGF-A, VEGF-C, VEGFR-3, neuropilin-2, and Notch signaling in mediating sprout formation (9, 24). Our results demonstrate that the 3D sprouting of LECs into the collagen hydrogel (Movie S1) is morphologically similar to in vivo vessel sprouting as recently depicted in the mouse retina (25). We used a combination of VEGF-A, bFGF and S1P to promote lymphatic sprout formation since these factors are involved in pathological tumor and lymph node lymphangiogenesis (26, 27), were previously validated in vitro (28), and yielded a more pronounced sprout formation in our assay than the individual growth factors. An advantage of our 3D assay is the automated image acquisition and analysis, which resolves these bottlenecks of conventional high-throughput screens. This also renders manual user intervention unnecessary, thereby providing a shortlist of screening hits whose selection is independent from interpretation by the experimentalist. Further advantages of this assay with regard to high-throughput screens are the short response time of 24 h, the straightforward experimental one-step

procedure after compound addition, the ability to provide dozens of bead sprouting sources per well (thereby increasing the number of internal replicates), the ability to detect sprouts horizontally and vertically in all levels, the compatibility with the 96-well format and the reliable separation of positive and negative controls. A potential weakness of the assay is our finding that dead cells, that are detached from the beads after treatment with cytotoxic drugs, are sometimes misinterpreted by the algorithm as sprouts and thus might occasionally lead to false negative results in the inhibitor screen. It is of interest that we have also successfully used this assay to quantify the sprout formation by immortalized murine LECs (kindly provided by Dr. Cornelia Halin, ETH Zurich), indicating the potential use for screens with genetically modified murine LECs as well as for phenotype rescue studies. The assay is also compatible with blood vascular ECs, enabling comparative studies with LECs. Our finding that the bead assay and its automated image acquisition and analysis could be adapted to a tumor cell setting will allow future screens with focused compound libraries to identify inhibitors of cancer cell invasion.

There have been previous in vivo phenotypic screens for inhibitors of blood vascular angiogenesis in zebrafish (29, 30) and *Xenopus* tadpoles (31); the latter also investigated the initial embryonic development of the lymphatic system. While such in vivo screening systems integrate all physiological processes and the completeness of a whole organism, they have some potential disadvantages compared to reductionist in vitro screens. First, test

compounds do not have direct access to their target but are resorbed, metabolized, and pharmacokinetically distributed. Therefore, potential lead structures might become false negatives—e.g., as compounds with a low $\log P$ such as U0126 (identified in this study) are less likely absorbed (32)—and there is not necessarily a correlation between compound concentrations in the medium and inside the zebrafish larva (33). Second, the drug effects can be conveyed by other cell types or can be altered by the immune system (34), potentially hampering attribution of a primary effect and aggravating retrospective target identification. Third, these vertebrate model systems are evolutionary distinct from human, and pharmacological responses sometimes differ tremendously between species as close as mammals; e.g., cytochrome P450 metabolism (35). Fourth, most phenotypic readouts in whole animal screens still depend on visual inspection (29, 31), thereby limiting throughput and introducing a potential bias.

The two replicate screenings of the (LOPAC)^{1280} for inhibitors of lymphangiogenic sprouting yielded a top hit rate of 2.4%, identifying 31 compounds with inhibition of at least 20% in both replicates. Besides the 10 cytotoxic compounds, we found nine top hits previously linked to angiogenesis, such as indirubin-3′-oxime and SU 5416. Interestingly, 54.8% (17 compounds) of the top hits had already shown to induce a vascular phenotype in a recent *Xenopus* tadpole screen, including the adenosine A1 receptor antagonist 7-chloro-4-hydroxy-2-phenyl-1,8-naphthyridine, whose anti-lymphangiogenic activity was later confirmed in a mouse lymphangiogenesis assay in vivo (31).

There are seven MAPKKs in humans that can be blocked with MEK inhibitors (11). Among the four major MAPK pathways, MEK1/2 has been shown to activate only ERK1/2, a major regulator of cell proliferation, survival, differentiation, motility, and angiogenesis that is activated by many growth factors and cytokines through activation of all three receptor classes (11). We found that the MEK inhibitor U0126, identified in our primary screen as a sprouting inhibitor, blocked lymphangiogenic sprouting in a dose-dependent manner with a minimal effective concentration of 1 μM. As U0126 also blocks MEK5 (11), we compared the inhibitory activity of MEK1/2 versus MEK5 selective inhibitors. As shown in biochemical assays, the tested inhibitors RDEA 119 and BIX 02189 have a comparable, low nanomolar inhibitory activity for their targets with IC_{50} values of 19 nM/47 nM on MEK1/2 (36), and 1.5 nM on MEK5 (37), respectively. Nevertheless, we found that the MEK1/2 inhibitor RDEA 119 was approximately 100 times more potent than the MEK5 inhibitor BIX 02189 in the sprouting assay. This result suggests that lymphangiogenic sprouting inhibition by U0126 is mediated by inhibition of MEK1/2. Mechanistically, we found that U0126 fully prevented ERK1/2 phosphorylation in LECs. Surprisingly, U0126 did not inhibit LEC proliferation at concentrations below 30 μM, suggesting that the MEK1/2-ERK1/2 axis plays a more important role in lymphangiogenic sprouting than in LEC proliferation.

It is of interest that U0126 was not identified as a hit in two previous developmental lymphangiogenesis screens in *Xenopus* tadpoles (31) and zebrafish (30). This is likely due to its low $\log P$ value of -1.07, which might have prevented efficient resorption from the media (32). Our finding that U0126 potently inhibited adult lymphangiogenesis in an established in vivo assay that partially mimics the tumor microenvironment, namely the mouse Matrigel plug assay loaded with VEGF, bFGF, and S1P, might provide an additional rationale for the use of MEK1/2 inhibitors in cancer therapy. As several major pharmaceutical companies are currently developing MEK1/2 inhibitors for anti-tumor therapy (11), it would be of interest to also investigate tumor lymphangiogenesis in these studies.

Statins are widely used for the treatment of dyslipidemia. They reduce low-density lipoprotein (LDL) levels in the plasma by inhibiting the 3-hydroxy-3-methylglutaryl-coenzyme A (HMG-CoA) reductase (HMGCR) and thereby cholesterol synthesis

(38). Recently, there has been increasing interest in their effects on cancer development (38). The hypothesis that statins might promote the risk for cancer development was not supported in the rosuvastatin/JUPITER trial (39). On the contrary, statin use was found to be associated with a reduced risk of prostate (40) and colorectal cancer (41). Statins have recently been found to inhibit HUVEC proliferation (16), spheroid sprouting (19) and intersegmental vessel growth in zebrafish embryos (29). In contrast to angiogenesis, the effect of statins on lymphangiogenesis and lymphangiogenic sprouting had not been investigated yet. Based on our preliminary identification of mevastatin as a potential lymphatic sprouting inhibitor, we tested additional statins, namely lovastatin, simvastatin, and atorvastatin. Our observations revealed that simvastatin was the most potent lymphatic sprouting inhibitor and, importantly, also strongly inhibited lymphangiogenesis in two independent experimental in vivo models of postnatal lymphatic vessel growth, namely the mouse Matrigel plug assay and the mouse cornea suture placement assay. The administered simvastatin dose of 2 mg/kg body weight was markedly lower than the dose of 5 mg/kg body weight utilized in recent angiogenesis animal studies (42, 43). Since our results indicate simvastatin as an inhibitor of pathological lymphangiogenesis, it would be of interest to investigate whether cancer patients on statin therapy might have a better prognosis due to decreased tumor lymphangiogenesis and metastasis (3, 6). Indeed, a recent publication indicates that patients on statin therapy develop fewer cancers and have a better prognosis once cancers have been diagnosed (44).

Regarding the mechanism of action of simvastatin, our findings indicate that simvastatin does not affect the phosphorylation of VEGFR-2 and ERK1/2, but instead acts via inhibition of HMGCR, which is expressed by LECs. This leads to decreased isoprenoid production, localization of Rac1 to the plasma membrane, and sprouting—in agreement with recent studies in blood vascular endothelium (42, 43, 45)—which can be rescued by supplementation with HMGCR products.

Materials and Methods

Cell Culture of Primary Lymphatic Endothelial Cells. Human dermal microvascular LECs were isolated from neonatal human foreskin as described (12) and were cultured on collagen (50 μg/ml, Advanced BioMatrix) coated plates in endothelial basal medium (EBM, Lonza), 20% FBS (Gibco), 1% antibiotic/antimycotic solution (Gibco), 4 mM L-glutamine (Gibco), 25 μg/ml cAMP (Sigma), and 10 μg/ml hydrocortisone (Sigma) at 37 °C in a humidified environment enriched with 5% CO_2.

Phenotype-based Screening Assay of Lymphangiogenic Sprouting. Rehydrated gelatin-covered cytodextran microcarrier beads (Sigma) were coated in suspension with LECs for 4 h under continuous stirring at a ratio of 1:40 (beads:cells) and incubated for another 48 h before use. Fully LEC-covered beads were labeled with 2 μM cell tracker green (CTG, Invitrogen) for 30 min, embedded into collagen type I hydrogels (1 mg/ml, Advanced BioMatrix) containing 2 μM sphingosine-1-phosphate (Avanti Polar Lipids) in black clear-bottom 96-well plates (Corning), cast for 1 h, and incubated with EBM containing 20% FBS, 40 ng/ml recombinant human VEGF-A165 (R&D Systems), and 40 ng/ml bFGF (R&D systems) for 24 h at 37 °C. Plates were fixed with 1% paraformaldehyde (Sigma) and imaged on an automated epifluorescence microscope MD ImageXpress micro 2 (Molecular Devices), equipped with a 4x 0.2 NA Plan Apo objective (Nikon), a 300W Xenon lamp (Sutter), a Roper CoolSnap HQ camera (Roper Scientific), and a 488 nm excitation FITC filter set. For dose response curves, selected compounds from the primary screen were tested in quintuplicates at concentrations of 0.01, 0.1, 1, 2.5, and 5 μM with identical assay conditions.

Analysis, Data Representation and Statistics. Images were processed and automatically analyzed for sprout number/bead with our software SproutCounter (*SI Materials and Methods*). The sprout number per bead data were normalized as percentage activity compared to the negative control (DMSO vehicle). Sunitinib (5 μM), omission of the lymphangiogenic stimulants, and vehicle DMSO served as a positive control, baseline activity control, and negative control, respectively. These intraplate controls were placed in columns 2

and 11 of each 96-well assay plate in quadruplicates. Calculations and graph plotting were prepared in Excel 2011 (Microsoft) and Prism 5.0 d (Graphpad), and results were plotted as bar graphs with standard error of the mean (SEM). All experiments were repeated at least two times ($n \geq 3$) and representative graphs are shown. Outliers were identified with the Grubb's test with alpha = 0.05 by Prism 5.0 d (Graphpad), and removed. The screening assay's "signal-to-noise ratio" (S:N) for each plate was calculated from equation (1) and expressed as mean with SEM for both replicates of the screen.

$$S:N = \frac{\text{mean(pos.control)} - \text{mean(neg.control)}}{\sqrt{\text{sd(pos.control)}^2 + \text{sd(neg.control)}^2}} \quad [1]$$

For statistical analysis, one-way ANOVA was performed in R [R Foundation for Statistical Computing (46)] for retrieving residuals and parameter estimation. Normal data distribution was confirmed quantitatively with a Shapiro-Wilk test ($p > 0.05$) in R. Estimation of statistically significant differences between the negative control and each treatment condition was achieved with a simple "contrast" analysis in R resulting in p-values (based on an F-distribution). For pairwise comparisons of sprouting inducers (Fig. 2C), proliferation assays (Fig. 4 B and C) and Rac1 activation (Fig. 4G) a Student t-test was used after confirming normal distribution with the Shapiro-Wilk test ($p < 0.05$). For the cornea assay analysis of lymphatic vessel coverage, a Mann-Whitney test was used for pairwise comparison. For all statistical analyses, p-values are indicated as follows: *<0.05, **<0.01, ***<0.001. All figures were generated using Illustrator CS5 version 15.0.2 (Adobe).

Immunofluorescent Staining of Beads and Laser Scanning Confocal Microscopy. LEC-coated beads were prepared and CTG labeled as described above, then fixed with 2% paraformaldehyde and blocked with 5% FBS (Gibco), 0.2% BSA (Sigma) for 1 h at room temperature. Primary mouse anti-human CD31 antibody (Dako) was applied for 1 h at room temperature, followed by secondary goat anti-mouse Alexa 594 conjugated antibody (Invitrogen) and Hoechst dye (Invitrogen) for 30 min at room temperature. 3D reconstructions of beads were acquired on a Leica SP2 AOBS (Leica) in 102 z-sections at 1.3 μm step size with a 20x N PL 0.4 objective and visualized with Imaris software (Bitplane).

Chemical Compounds. The Library of Pharmacologically Active Compounds ((LOPAC)[1280], Sigma) was screened at 5 μM compound concentration in the sprouting assay. Upon hit identification, all compounds were reordered as powders from the following vendors: sunitinib (LC Laboratories), BIX 02189 (Selleck Chemicals), RDEA 119 (Active Biochemicals), U0126 (Tocris), mevastatin, simvastatin, lovastatin, atorvastatin, and diphenyleneiodonium chloride (all from Sigma). All compounds were dissolved in DMSO at 10 mM and aliquoted at 1 mM. A final DMSO concentration of 0.5% in cell culture and of 5% in vivo studies was not exceeded. The negative controls contained the same percentage of vehicle. For the HMGCR inhibition rescue studies, 100 μM mevalonate, 10 μM farnesyl pyrophosphate, and 10 μM geranylgeranyl pyrophosphate (all from Sigma) were used.

Membrane/Cytosol Fractionation. After treatment with VEGF-A, bFGF (both at 40 ng/ml), and 2 μM S1P in complete medium for 24 h, LECs were lysed in a hypotonic phosphate-buffered saline (PBS) solution containing 1 mM $MgCl_2$, 1 mM $CaCl_2$, 1 mM phenylmethanesulfonyl fluoride, and protease inhibitor cocktail (Roche) by 20 strokes through a 25G needle. Nuclei were removed by centrifugation at $2000 \times g$ before the membranes were separated from the

cytosolic supernatant by ultracentrifugation (Beckman Coulter) at $100,000 \times g$ for 30 min at 4 °C. Samples were dissolved in Hepes buffer supplemented with 10% glycerol, 1 mM $MgCl_2$, 1 mM $CaCl_2$, 1 mM PMSF and protease inhibitor cocktail (Roche).

SDS-PAGE and Immunoblotting. Proteins were denatured by boiling in Laemmli buffer, resolved in 8% or 10% polyacrylamide gels (Bio Rad), and transferred to polyvinylidene fluoride membranes (Millipore) that were blocked in 5% nonfat dry milk Tris buffered saline (TBS, Sigma) containing 0.1% Tween-20 (Sigma) for 2 h at room temperature or overnight at 4 °C. Subsequently, membranes were incubated with antibodies against VEGFR-3 (1:500, SantaCruz, sc-321), (p1175)VEGFR-2 (1:1000, Cell Signaling, #2478), ERK1/2 (1:1000, Cell Signaling, #4695), (p202/p204)ERK1/2 (1:1000, BD, #612358), β-actin (1:3000, Abcam, ab8227), or Rac1 (1:500, Millipore, # 05-389) for 1–2 h at room temperature or at 4 °C overnight, followed by horseradish peroxidase-coupled anti-mouse or anti-rabbit antibodies (both GE Healthcare, 1:3000 and 1:5000, respectively) in 1% nonfat dry milk TBS solution containing 0.1% Tween-20.

For reprobing of similar sized proteins, membranes were stripped for 20 min at 52 °C with TBS containing 2% SDS and β-mercaptoethanol. Bands were visualized with the ECL Plus Detection kit (GE Healthcare) and chemiluminescence films (Kodak).

Rac1 Activation Level Detection. LECs were treated appropriately, harvested, and amounts of activated GTP-bound Rac1 were quantified with the G-LISA Biochem Kit (Cytoskeleton) according to the vendor's protocol.

Proliferation Assays. Subconfluent LECs on 50 μg/ml collagen type I (Advanced BioMatrix) coated black clear-bottom 96-well plates (Corning) were incubated with EBM containing 20% FBS, 40 ng/ml recombinant human VEGF-A165 (R&D Systems), 40 ng/ml bFGF (R&D Systems), and 2 μM sphingosine-1-phosphate (Avanti Polar Lipids) in the presence of increasing drug dosages for 48 h at 37 °C. After washing, cells were incubated with 0.1 mg/ml 4-methylumbelliferyl enanthate (Sigma) in the dark for 1 h at 37 °C before measuring fluorescence (355 nm ex/460 nm em) on a SpectraMAX GeminiEM plate reader (Molecular Devices).

In Vivo Matrigel Plug Assays and In Vivo Cornea Assays. In vivo assays were performed largely as described (12, 15). For details, see *SI Material and Methods*.

1. Christiansen A, Detmar M (2011) Lymphangiogenesis and cancer. *Genes Cancer* 2:1146–1158.

2. Dadras SS, et al. (2003) Tumor lymphangiogenesis: A novel prognostic indicator for cutaneous melanoma metastasis and survival. *Am J Pathol* 162:1951–1960.

3. Hirakawa S, et al. (2005) VEGF-A induces tumor and sentinel lymph node lymphangiogenesis and promotes lymphatic metastasis. *J Exp Med* 201:1089–1099.

4. Kim M, et al. (2010) CXCR4 signaling regulates metastasis of chemoresistant melanoma cells by a lymphatic metastatic niche. *Cancer Res* 70:10411–10421.

5. Jurisic G, Detmar M (2009) Lymphatic endothelium in health and disease. *Cell Tissue Res* 335:97–108.

6. Skobe M, et al. (2001) Induction of tumor lymphangiogenesis by VEGF-C promotes breast cancer metastasis. *Nat Med* 7:192–198.

7. Hirakawa S, et al. (2007) VEGF-C-induced lymphangiogenesis in sentinel lymph nodes promotes tumor metastasis to distant sites. *Blood* 109:1010–1017.

8. Caunt M, et al. (2008) Blocking neuropilin-2 function inhibits tumor cell metastasis. *Cancer Cell* 13:331–342.

9. Zheng W, et al. (2011) Notch restricts lymphatic vessel sprouting induced by vascular endothelial growth factor. *Blood* 118:1154–1162.

10. Swinney DC, Anthony J (2011) How were new medicines discovered? *Nat Rev Drug Discov* 10:507–519.

11. Frémin C, Meloche S (2010) From basic research to clinical development of MEK1/2 inhibitors for cancer therapy. *J Hematol Oncol* 3:8.

12. Hirakawa S, et al. (2003) Identification of vascular lineage-specific genes by transcriptional profiling of isolated blood vascular and lymphatic endothelial cells. *Am J Pathol* 162:575–586.

13. Shin JW, Huggenberger R, Detmar M (2008) Transcriptional profiling of VEGF-A and VEGF-C target genes in lymphatic endothelium reveals endothelial-specific molecule-1 as a novel mediator of lymphangiogenesis. *Blood* 112:2318–2326.

14. Jurisic G, Iolyeva M, Proulx ST, Halin C, Detmar M (2010) Thymus cell antigen 1 (Thy1, CD90) is expressed by lymphatic vessels and mediates cell adhesion to lymphatic endothelium. *Exp Cell Res* 316:2982–2992.

15. Yuen D, Pytowski B, Chen L (2011) Combined blockade of VEGFR-2 and VEGFR-3 inhibits inflammatory lymphangiogenesis in early and middle stages. *Invest Ophthalmol Vis Sci* 52:2593–2597.

16. Chong CR, et al. (2007) Inhibition of angiogenesis by the antifungal drug itraconazole. *ACS Chem Biol* 2:263–270.

Schulz et al.

17. Evensen L, Micklem DR, Link W, Lorens JB (2010) A novel imaging-based high-throughput screening approach to anti-angiogenic drug discovery. *Cytometry A* 77:41–51.

18. Sanz L, et al. (2002) Development of a computer-assisted high-throughput screening platform for anti-angiogenic testing. *Microvasc Res* 63:335–339.

19. Kalén M, et al. (2009) Combination of reverse and chemical genetic screens reveals angiogenesis inhibitors and targets. *Chem Biol* 16:432–441.

20. Bruyère F, et al. (2008) Modeling lymphangiogenesis in a three-dimensional culture system. *Nat Methods* 5:431–437.

21. Adams RH, Alitalo K (2007) Molecular regulation of angiogenesis and lymphangiogenesis. *Nat Rev Mol Cell Biol* 8:464–478.

22. Nehls V, Drenckhahn D (1995) A novel, microcarrier-based in vitro assay for rapid and reliable quantification of three-dimensional cell migration and angiogenesis. *Microvasc Res* 50:311–322.

23. Nakatsu M, Hughes C (2008) An optimized three-dimensional in vitro model for the analysis of angiogenesis. *Methods Enzymol* 443:65–82.

24. Xu Y, et al. (2010) Neuropilin-2 mediates VEGF-C-induced lymphatic sprouting together with VEGFR3. *J Cell Biol* 188:115–130.

25. Pitulescu ME, Schmidt I, Benedito R, Adams RH (2010) Inducible gene targeting in the neonatal vasculature and analysis of retinal angiogenesis in mice. *Nat Protoc* 5:1518–1534.

26. Kerjaschki D, et al. (2011) Lipoxygenase mediates invasion of intrametastatic lymphatic vessels and propagates lymph node metastasis of human mammary carcinoma xenografts in mouse. *J Clin Invest* 121:2000–2012.

27. Yoon CM, et al. (2008) Sphingosine-1-phosphate promotes lymphangiogenesis by stimulating S1P1/Gi/PLC/Ca^{2+} signaling pathways. *Blood* 112:1129–1138.

28. Bayless KJ, Kwak H-I, Su S-C (2009) Investigating endothelial invasion and sprouting behavior in three-dimensional collagen matrices. *Nat Protoc* 4:1888–1898.

29. Wang C, et al. (2010) Rosuvastatin, identified from a zebrafish chemical genetic screen for antiangiogenic compounds, suppresses the growth of prostate cancer. *Eur Urol* 58:418–426.

30. Tran TC, et al. (2007) Automated, quantitative screening assay for antiangiogenic compounds using transgenic zebrafish. *Cancer Res* 67:11386–11392.

31. Kälin RE, Bänziger-Tobler NE, Detmar M, Brändli AW (2009) An in vivo chemical library screen in Xenopus tadpoles reveals novel pathways involved in angiogenesis and lymphangiogenesis. *Blood* 114:1110–1122.

32. Peterson RT, Fishman MC (2004) Discovery and use of small molecules for probing biological processes in zebrafish. *Methods Cell Biol* 76:569–591.

33. Berghmans S, et al. (2008) Zebrafish based assays for the assessment of cardiac, visual and gut function: Potential safety screens for early drug discovery. *J Pharmacol Toxicol Methods* 58:59–68.

34. Santos AF, et al. (2008) Angiogenesis: An improved in vitro biological system and automated image-based workflow to aid identification and characterization of angiogenesis and angiogenic modulators. *Assay Drug Dev Technol* 6:693–710.

35. Gibbs RA, et al. (2004) Genome sequence of the Brown Norway rat yields insights into mammalian evolution. *Nature* 428:493–521.

36. Iverson C, et al. (2009) RDEA119/BAY 869766: A potent, selective, allosteric inhibitor of MEK1/2 for the treatment of cancer. *Cancer Res* 69:6839–6847.

37. Tatake RJ, et al. (2008) Identification of pharmacological inhibitors of the MEK5/ERK5 pathway. *Biochem Biophys Res Commun* 377:120–125.

38. Hindler K, Cleeland CS, Rivera E, Collard CD (2006) The role of statins in cancer therapy. *Oncologist* 11:306–315.

39. Ridker PM, et al. (2008) Rosuvastatin to prevent vascular events in men and women with elevated C-reactive protein. *N Engl J Med* 359:2195–2207.

40. Farwell WR, D'Avolio LW, Scranton RE, Lawler EV, Gaziano JM (2011) Statins and prostate cancer diagnosis and grade in a veterans population. *J Natl Cancer Inst* 103:885–892.

41. Poynter JN, et al. (2005) Statins and the risk of colorectal cancer. *N Engl J Med* 352:2184–2192.

42. Park H-J, et al. (2002) 3-hydroxy-3-methylglutaryl coenzyme A reductase inhibitors interfere with angiogenesis by inhibiting the geranylgeranylation of RhoA. *Circ Res* 91:143–150.

43. Singh NK, Kundumani-Sridharan V, Rao GN (2011) 12/15-Lipoxygenase gene knockout severely impairs ischemia-induced angiogenesis due to lack of Rac1 farnesylation. *Blood* 118:5701–5712.

44. Fröhlich GM, et al. (2012) Statins and the risk of cancer after heart transplantation. *Circulation* 126:440–447.

45. Vincent L, et al. (2001) Inhibition of endothelial cell migration by cerivastatin, an HMG-CoA reductase inhibitor: Contribution to its anti-angiogenic effect. *FEBS Lett* 495:159–166.

46. Team RDC (2008) R: A Language and Environment for Statistical Computing. (R Foundation for Statistical Computing, Vienna, Austria).